Energy materials

Sputtered titanium nitride films as pseudocapacitive electrode for on chip micro-supercapacitors

Jing Shi[1,*] , Bailing Jiang[1,*], Cong Li[2], Zheng Liu[1], and Fangyuan Yan[1]

[1] School of Materials Science, Xi'an University of Technology, Xi'an 710048, People's Republic of China
[2] School of Materials Science and Engineering, Xi'an Jiaotong University, Xi'an 710049, People's Republic of China

ABSTRACT

Micro-supercapacitor is one of the most promising types of autonomous, miniaturized and compact electrochemical devices currently used in the Internet of Things (smart and self-powered sensors). Micro-supercapacitor is mainly based on advanced thin-film technology to prepare high-performance thin film electrodes. However, the deposition of electroactive film electrode materials on large-scale substrates remains a challenge. In this paper, a bifunctional pseudocapacitive electrode material titanium nitride was deposited on Si substrate by reactive direct current magnetron sputtering. To obtain the TiN film electrode with excellent electrochemical performance, the intra-column porosity of the TiN film was fine-tuned at the nanoscale, the surface stoichiometric ratio of the film was analyzed, and the relationship between the specific surface area and the areal/volume capacitance of the film was explored. The results show that by fine tuning the working pressure in the sputtering process, films with high intra-column porosity can be obtained; the electrochemical properties of TiN films with stoichiometric ratio of 1:1 and over-stoichiometric ratio are better than those of sub-stoichiometric ratio; and the Gwyddion image analysis technique evaluates the specific surface area of the film surface and shows that the areal capacitance of the film increases linearly with the specific surface area of the film. In addition, the areal capacitance retention of TiN films with a thickness of 626 nm is still as high as 91.4% after 10,000 cycles in the K_2SO_4 electrolyte solution. These results provide direction for the study of other nitrides film electrode materials.

Introduction

With the in-depth research on wireless sensor networks, self-powered sensor networks have become a key field of world economic development [1]. The introduction of wireless sensor networks into various application fields such as home appliance automation, traffic monitoring, human health control and environmental monitoring plays an important role in our daily life and industrial progress [2–5]. However, the power consumption of a single device in the wireless self-powered network is large, the large number and small size of sensors make it difficult to replace the battery, and the replaced battery is not friendly to the environment [1]. Therefore, researchers are committed to the research on the independence, sustainability, maintenance-free and continuous operation of equipment and systems, hoping to obtain energies from environmental energy (intermittent and unstable) and smoothly output this energy through energy storage devices to realize the self-power supply of sensors [6]. The micro-lithium ion batteries and micro-supercapacitors are the satisfying candidates for these energy storage devices. In recent decades, lithium-ion batteries have successfully promoted the vigorous development of electronic products. However, the short charge and discharge times and low power density of the lithium-ion battery hinder the service life of the sensor. Micro-supercapacitors for electrochemical energy storage have higher power density [7–11], and longer lifetime than Li-ion batteries [12–15]. They are more suitable for some self-powered networks than lithium-ion batteries.

On-chip micro-supercapacitor refers to the micro-supercapacitor integrated by designing microelectronic chips on a silicon substrate. Common micro-supercapacitor electrode materials include carbon materials with charge storage mechanism dominated by electric double layers (EDLC), mainly including porous surface carbon nanotubes (CNTs) with staggered networks, activated carbon, graphene oxide, etc. [16]. Electrodes made of carbon material with a large specific surface area have problems such as poor adhesion performance and low energy density, which can not satisfy the peak power of self-powered network system. Another common electrode material is the electrode material with pseudo capacitance, which is mainly composed of metal oxides. Their energy density is at least one order of magnitude higher than that of EDLC through the rapid redox reaction of electroactive materials in the material [16, 17]. The disadvantage of metal oxide electrodes is their poor electronic conductivity and unreliable stability over a long period. At present, metal nitrides have been widely concerned because they have better conductivity and better persistence than metal oxides [18].

Titanium nitride (TiN) with high conductivity (4.0×10^3 and 5.5×10^4 S cm^{-1}) is an electrode material that can quickly transmit and effectively collect charges, has strong adhesion to the substrate, is corrosion resistant (adapt to corrosive electrolyte) and is a good diffusion barrier [19, 20]. TiN electrode material is often used in on-chip micro-supercapacitor devices [21], which requires accurate and controllable load. The most common methods for synthesizing TiN electrodes with different nanoforms include: (1) The prepared metal oxide is used to obtain a nitride electrode at high temperature in nitrogen or ammonia environment [22, 23]. (2) TiN powder electrode synthesized by hydrothermal methods [24]. These wet prepared TiN electrodes often increase the peripheral resistance [25] due to the poor connection between the electrode and the collector, and are difficult to be compatible with lithography technology and cannot be applied to wafer devices. On the other hand, the preparation of TiN powder electrodes cannot ensure the minimization of the total device size [26], mainly because devices with interdigital structure require that the minimum distance between electrodes should be at the sub millimeter level.

TiN electrode prepared by physical vapor deposition (PVD) has the advantages of controllable thickness, good adhesion and a certain stoichiometric ratio. And it is a good alternative to solve the above problems [27–29]. Achour et al. [30] obtained a TiN thin film electrode by DC magnetron sputtering, which had a brilliant volume capacitance of 146.4 F cm^{-3}. In addition, they thermally annealed TiN films [31], and found that the Ti–O–N bond on the surface of the annealed films increased, making the areal capacitance of TiN films annealed at 500 °C three times that of non annealed films. The results show that the surface chemical composition of TiN films has an important influence on the supercapacitor properties of TiN films. Recently, some research groups have studied that the working pressure

during magnetron sputtering has a significant effect on the specific capacitance of TiN film[32, 33]. Specifically, when the working pressure is increased from 0.3 Pa to 1.3 Pa, the area capacitance of TiN film electrode is increased from 0.3 to 4.7 mF cm^{-2} [33]. Their researches mainly focused on obtaining TiN electrode with an excellent performance by adjusting sputtering deposition time and sputtering power, but there was no systematic report on the relationship between porosity, thickness and S_e of TiN film electrodes. The working pressure, nitrogen flow rate and deposition time in the deposition process have great effects on the porosity (specific surface area) of the film, the active material composition of the electrode material and its load. However, the porosity of the film is mainly achieved by adjusting the working pressure. When the stoichiometric ratio of Ti/N is 1, the thin film has the highest conductivity, and the electrode with excellent performance can be obtained by controlling the nitrogen flow [31], and the mass loading of the active material of the film electrodes can be obtained by controlling the deposition time.

In this paper, the effects of controlling the porosity of thin films, the chemical composition of films and the mass loading of films on the supercapacitor properties of TiN film electrodes are emphasized. The functional relationship between the film thickness and its surface-specific surface area is analyzed, and the relationship between the specific surface area in the film and the electrode areal capacitance of TiN film is discussed. These results can be used as an indication of the effect of deposition conditions on the structure and electrochemical properties of other nitride layers.

Experimental procedures

TiN film deposition: The monocrystalline silicon wafer with (100) crystal orientation was cut into 2 mm × 2 mm. Washed the Si sheets in acetone, alcohol and deionized water for cleaning for 15 min, to remove organic pollutants and dust on the surface of the Si wafer. Then, it is dried in a nitrogen atmosphere and put into a magnetron sputtering chamber. Before sputtering, the vacuum in the sputtering chamber was maintained at 3.0×10^{-4} torr. Before sputtering, the sputtering gas Ar with a purity of 99.99% was introduced into the sputtering chamber, and the Ar flow was fixed at 26 sccm. The titanium

target (purity: 99.99%) current, bias voltage loaded on the substrate and pre-sputtering time were set to 0.05 A, −400 V and 20 min, respectively. The purpose of pre-sputtering was to remove the oxide layer on the target surface. At the beginning of the deposition, the reaction gas nitrogen with a purity of 99.99% was also introduced into the sputtering chamber. In the sputtering process, the target substrate distance was 120 mm and the rotation speed of the substrate was 5 rpm. The effects of working pressure, nitrogen flow rate and film thickness on the microstructure and supercapacitor properties of TiN films were studied. Figure 1 shows a schematic diagram of nanoporous TiN films prepared by DC magnetron sputtering.

Characterizations of deposited TiN films: The phase identification of TiN thin films was carried out by XRD instrument, the model is XRD-7000 s, and the sample detection angle range was 30–80°. The surface morphology and cross-section morphology of TiN films were analyzed with a JSM-6700F scanning electron microscope. The chemical composition and chemical bond types of the film surface were detected by X-ray photoelectron spectroscopy (AXIS ULTRA). After measurement, the binding energies were calibrated using the C 1 s peak (284.5 eV) [34].

The surface roughness of TiN film was examined under an atomic force microscope of Bruker HTZC-14014. The image analysis software Gwyddion (version 2.45, 2016) was used to analyze the maximum perimeter (L_p) and the specific surface area (S_e) of the grain projection under the three-dimensional morphology of TiN. L_p was defined as the length of the cylindrical/conical cylindrical boundary projection on the TiN film surface. Select three areas on the sample, which are 5×5 μm^2. 4×4μm^2 and 3×3 μm^2. The surface roughness and L_p are tested three times respectively, and then the average value of nine measurement results is obtained to ensure the accuracy of the value. The specific calculation methods were summarized in the previously published articles and will not be repeated here [35]. This method of calculating the specific surface area of TiN film was slightly lower than the actual value, mainly because it assumed that the grain was a perfect cylinder. However, this method can also be used to evaluate the relationship between specific surface areas and growth conditions.

Cyclic voltammetry (CV) and alternating current impedance (EIS) were measured on a CHI 660E electrochemical workstation with 0.5 M K_2SO_4. The
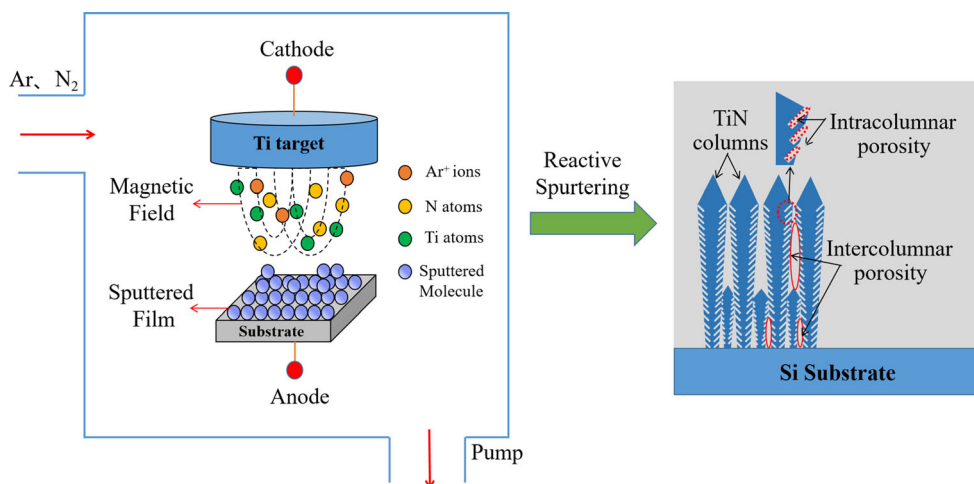
Figure 1 Schematic diagram of the nanoporous TiN film prepared by magnetron sputtering.

CV curves were the curves given after 10 cycles to ensure the stability and accuracy of the test. Platinum mesh electrode is used as counter electrode and Ag/AgCl electrode is used as reference electrode. The conductivity was acquired by converting the resistance of the film (measured by four probes) and the thickness of the film. Bruke UMT trilbolab equipment is used to test the adhesion of the films. The loading load was 60 N. The scratch morphology is observed by GX71 inverted metallographic microscope.

Result and discussion

Titanium nitride is used as the electrode plate of the micro-supercapacitor because it can be used as both a fluid collector and pseudocapacitor electrode with high efficiency. Therefore, during the sputtering process, the electrical and electrochemical performances of the films can be accurately controlled by adjusting the porosity in the TiN column, surface chemical composition and electroactive material mass loading. The change of porosity in the film column is closely related to the working pressure of the film preparation, and the chemical composition of the film surface also affects the electrochemical properties of the TiN film electrode. In addition, the mass loading of the electrode is increased by prolonging the sputtering time. Thus, a high-performance titanium nitride film electrode for supercapacitor can be prepared.

Influence of working pressure

In the sputtering process, the working pressure affects the shot peening effect of deposited atoms on the film surface, which affects the densification of the film. In this paper, the sputtering process is carried out at furnace temperature (T/T_m value is constant, T matrix temperature, T_m, material melting temperature, K), indicating that the film morphologies are in zone 1/T of Thornton [36]. The densification of the TiN thin films mainly realizes the local displacement of atoms on the atomic scale by changing the working pressure. TiN films were deposited under the conditions of working pressures of 0.98×10^{-3} torr, 1.2×10^{-3} torr and 1.5×10^{-3} torr with Ar:N$_2$ flow ratio of 26:6. The deposition time was maintained for 60 min.

Figure 2 shows SEM images of TiN films under various sputtering pressures. From the surface SEM images, the films show granular grains at 0.98×10^{-3} torr, and the agglomerated particles on the film surface increase and more pores appear on the surface at $1.2 \sim 1.5 \times 10^{-3}$ torr (Fig. 2a–c). A similar trend appears in the surface roughness of TiN films. The surface roughness of the film increases from 4.23 (0.98×10^{-3} torr) to 7.88 nm (1.5×10^{-3} torr) (Fig. 3b insert left axis), which provides contact points for the charge and facilitates the storage of the charge. From the cross-section SEM images (Fig. 2d –f), it can be observed that the thickness of the film increases from 626 nm (0.98×10^{-3} torr) to 795 nm (1.5×10^{-3} torr) with the increase of working pressure, which corresponds well to the increase of
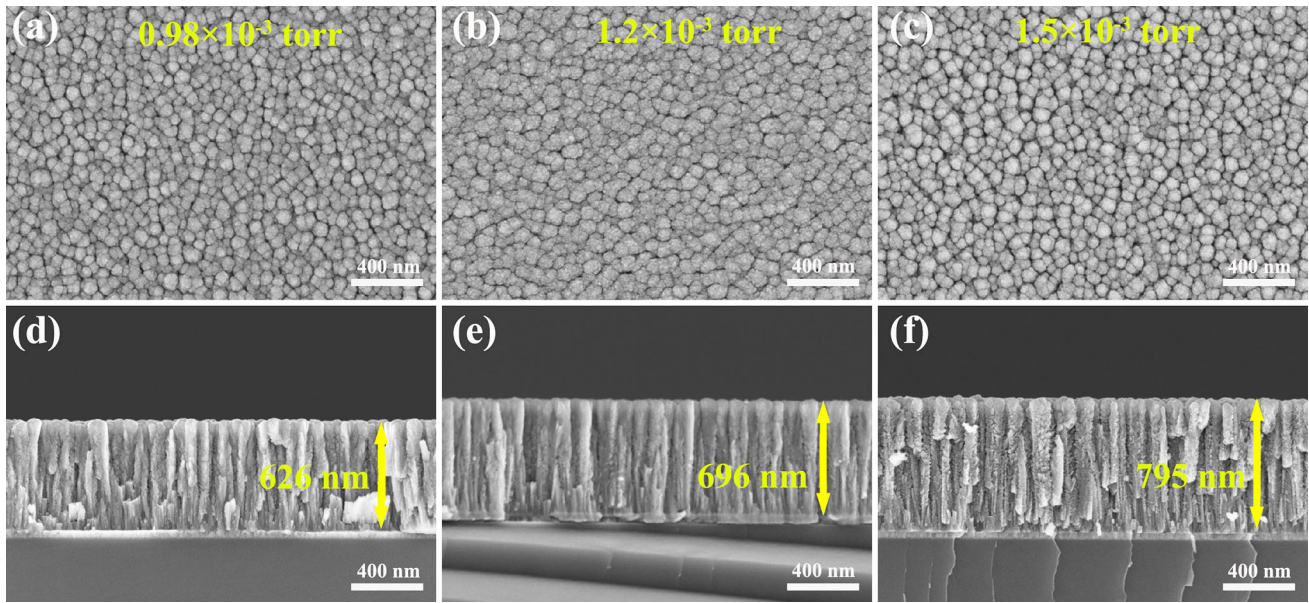
Figure 2 Surface and cross-section morphologies of TiN films at different working pressure, **a, d** 0.98×10^{-3} torr, **b, e** 1.2×10^{-3} torr, **c, f** 1.5×10^{-3} torr.
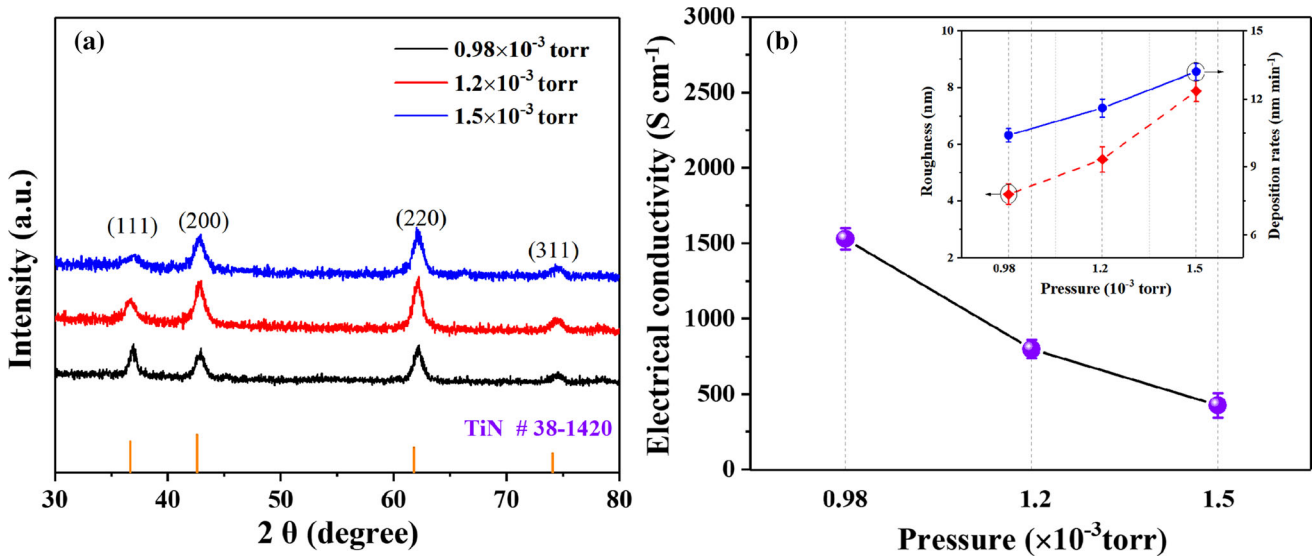

Figure 3 XRD patterns **a** and **b** changes of conductivity and deposition rate with the TiN films under different working pressure. (*Insert*) Roughness (*left axis*) and deposition rates (*right axis*) under different working pressure.

deposition rate (Fig. 3b insert right axis). In addition, the prepared TiN films all present columnar structure, and with the increase of working pressure, the columnar structure of TiN films presents "feather-like", indicating that there are a large number of pores in the films. Because the deposition rate of TiN films increases with the increase of working pressure, it shows that TiN atoms have no time to diffuse during the deposition process, resulting in "shielding effect" and leaving more porosity. Therefore, the increase of TiN working pressure during deposition provides more intra-column porosity (refers to the pores on a single column) and inter-column porosity (pores between columns) for TiN film electrode, increases the specific surface area of TiN film surface. This provides more contact points between TiN film electrode and electrolyte, thus increasing the storage capacity of charge.

Figure 3a displays the XRD patterns of TiN at different working pressure. The films have four reflection peaks (111), (200), (220) and (311), corresponding to TiN (JCPDS card no. 38–1420) with a FCC structure. The intensity of the two reflection peaks of films (111), (200) decreases with the increase of working pressure. While TiN films grow in the direction of (220) at higher working pressure of 1.5×10^{-3} torr.

Figure 3b shows the change of film conductivity with sputtering working pressure. From Fig. 3, as the working pressure increases, the conductivity of the TiN film decreases, which is due to the increase in the porosity of the TiN film. Specifically, the conductivity decreased from 1530 S cm^{-1} at 0.98×10^{-3} torr to 426 S cm^{-1} at 1.5×10^{-3} torr.

The chemical state of TiN film surface under different working pressure was analyzed by XPS. The high-resolution spectra of Ti 2p and N 1 s of TiN films under different working pressures are almost identical. The Ti 2p high-resolution spectrum peak can be divided into two typical peaks, namely Ti 2p$_{3/2}$ and Ti 2p$_{1/2}$. Taking Ti 2p$_{1/2}$ as an example, the

deconvolutions of Ti 2p$_{3/2}$ peaks exhibit that there are three compounds in TiN films under different working pressures, namely Ti−N, Ti−O−N and Ti−O chemical bonds, as shown in Fig. 4a. The corresponding binding energies of the three compounds are at 455.8 eV, 456.9 eV and 458.4 eV, respectively, and the binding energies of these three chemical bonds correspond to TiN, TiO$_x$N$_y$ and TiO$_x$ tin, tioxny and TiO$_x$ [37]. Correspondingly, the N 1 s fine spectrum can also be deconvoluted three compounds containing N, namely Ti−N−O, Ti−N and N−N chemical bonds, as shown in Fig. 4b, which exactly correspond to the three compounds of TiO$_x$N$_y$, TiN and adsorbed nitride (N−N), and their binding energies are 396.0 eV, 397.0 eV, 398.9 eV, respectively.

In order to further explore the chemical composition of TiN film surface during sputtering, the relative percentages of three functional groups under the high-resolution spectra of Ti 2p and N 1 s at different working pressures were calculated, as shown in Table 1. It can be seen from Table 1 that the
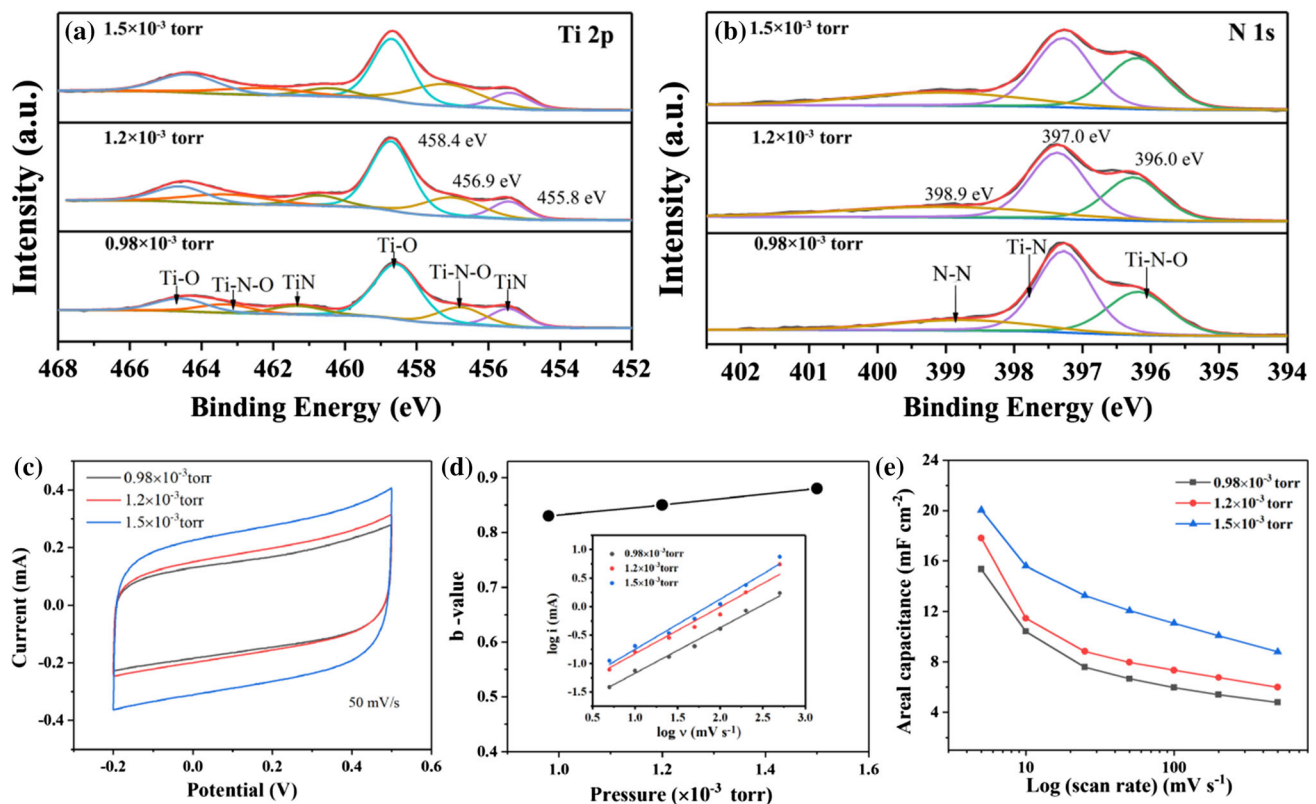

Figure 4 High-resolution spectra of Ti 2p and N 1 s in TiN films **a, b**. Electrochemical diagrams of TiN films. **c** Cyclic voltammetry curves of TiN films at a 50 mV s^{-1}. **d** The relationship between areal capacitance and log (scan rate). **e** The b value vs. the working pressure. (*Insert*) The current vs. log (scan rate).

Table 1 The chemical bond fraction (%) of Ti 2p and N 1 s

Working pressure (× 10^{-3} torr)	Ti 2p (%)			N 1 s (%)		
	Ti−N−O	Ti−N	Ti−O	Ti−N−O	Ti−N	N−N
0.98	32.14	31.80	36.06	32.88	37.55	29.57
1.2	33.69	29.73	36.58	34.65	33.84	31.51
1.5	35.13	27.82	37.05	35.29	32.46	32.25

deconvolution peaks Ti−N–O and Ti−N of Ti 2p and N 1 s high-resolution spectral peaks have the same change trend. From 0.98×10^{-3} torr to 1.5×10^{-3} torr, the relative content of Ti−N bond decreased, and the relative content of Ti−N–O bond increased from 32% to about 35%. The increase of the relative content of Ti−N–O can promote the pseudo capacitance of TiN film electrode [38]. In addition, the content of Ti–O bond under the high-resolution spectrum peak of Ti 2p also increases slightly, as shown in Table 1. The existence of Ti–O bond is related to more porosity in the column under high working pressure. This structure will absorb more incompletely purified mixed gas in the furnace chamber [30].

Figure 4c shows the CV curves of TiN films under different working pressures ($5 \sim 500$ mV s^{-1}). It can be observed from the figure that the shape of CV curves under different working pressures is similar to the rectangle, indicating that all TiN films have excellent charge storage properties. Moreover, the integral area of CV curves of the TiN film increases with the increasing working pressure. Therefore, with the increase of working pressure, the areal capacitance of TiN area increases. As the scanning speed is 10 mV s^{-1}, the areal capacitances of the films are 10.42 mF cm^{-2} 11.47 mF cm^{-2} and 15.60 mF cm^{-2}, respectively. The storage charge of TiN film is mainly through the "Faraday effect" of the TiN surface, including the electric double-layer storage capacitance formed near the surface and the phase change free pseudo capacitance on the surface. The specific reaction formula (1) is as follows:

$$TiN + K_2SO_4 \rightarrow TiN||K^+ + TiN - K^+ \tag{1}$$
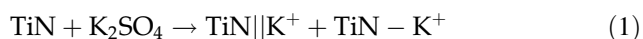
TiN | | K$^+$ represents electric double layer and TiN-K$^+$ represents pseudo capacitance mechanism. With the increase of deposition pressure, the surface roughness of TiN film increases and the pores in the column increase, which is conducive to providing high areal capacitance. In addition, studies have shown that the increase of nitrogen oxides on the film surface can also improve the areal capacitance of the film surface, which is mainly due to the charge storage of TiO$_x$N$_y$ on the TiN film electrode surface through continuous chemical adsorption of cations. The chemical formula (2) is as follows:

$$TiO_xN_y + K^+ + e^- \rightarrow \left(TiO_xN_y^- - K^+\right)_{surface} \tag{2}$$

To better understand the charge accumulation of TiN films, a power-law formula is introduced for analysis. The following formula (3) is given:

$$I = a \cdot v^b \tag{3}$$

where I is the current from the CV curve, (mA), v is the scanning rate (mV s^{-1}), and a and b are both constants. The b value is used to distinguish which electrochemical process is involved in the charge storage process of electrode materials. For the electrode with b value close to 0.5, such as battery type material, the electrode storage is dominated by pure diffusion limitation, and the b value close to 1 indicates that the electrode material is an ideal supercapacitor material, and the electrode mainly stores charge by pure capacitance or pseudo capacitance. From Fig. 4d, as the working pressure increases from 0.98 to 1.5×10^{-3} torr, the b value of TiN film electrodes increases from 0.83 to 0.88, indicating that the electrode working pressure of TiN electrode is between $0.98 \sim 1.5 \times 10^{-3}$ torr, the charge storage process is not limited by solid-state diffusion.

Influence of nitrogen flow rate

The surface composition of TiN film is an important parameter, which affects the electrical and electrochemical properties of TiN film electrodes to a great extent. Therefore, a series of TiN films with different N$_2$ flow rates were obtained by fixing the deposition working pressure (0.98×10^{-3} torr), deposition time (60 min) and argon flow rate (26 sccm) at room temperature. The changes in microstructures of TiN with nitrogen flow rates are shown in Fig. 5.
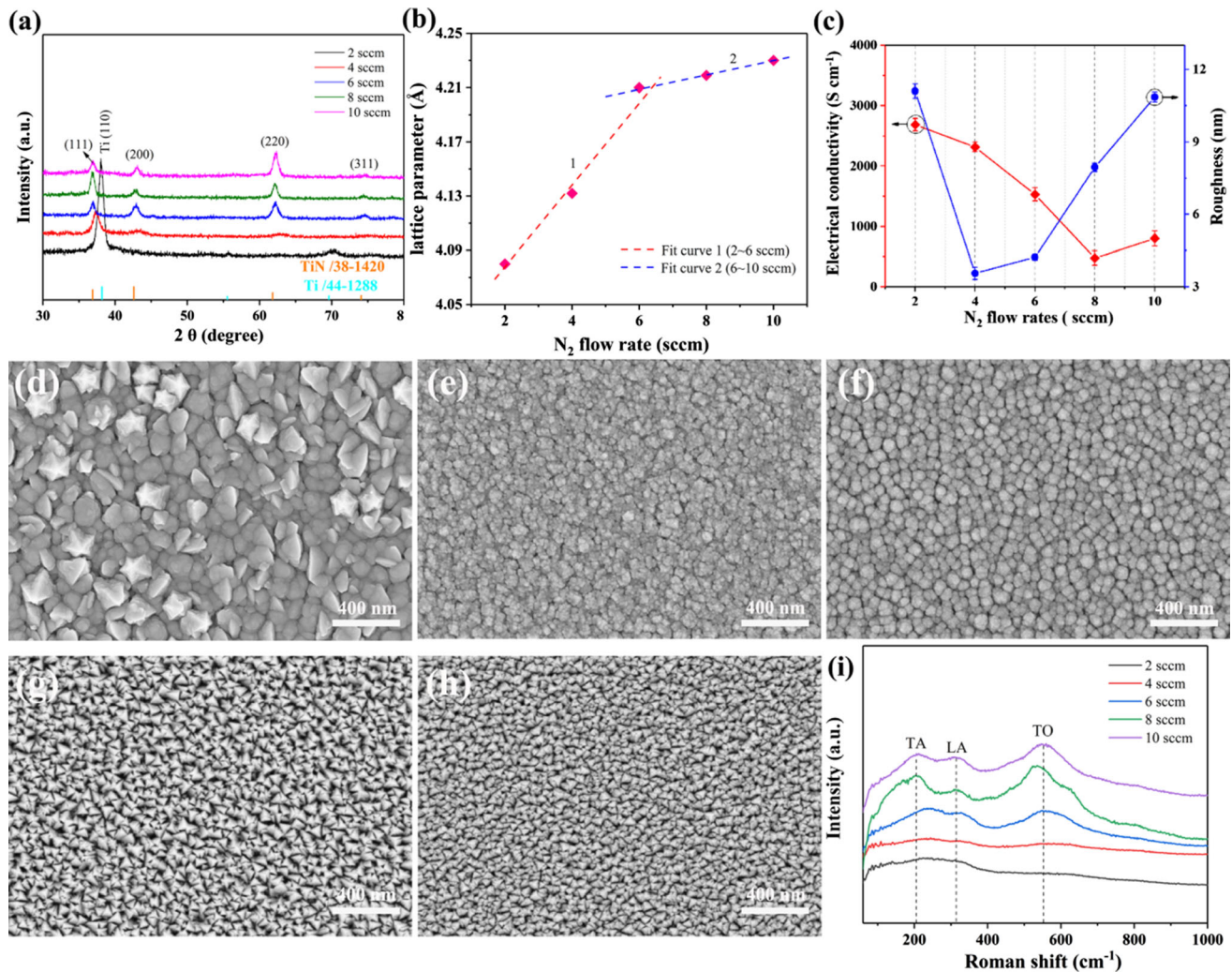
Figure 5 **a** XRD and **b** lattice constant diagrams of TiN films under different N_2 flow rates. **c** Changes in conductivity and deposition rate with the TiN films at different N_2 flow rates.

Surface morphologies of TiN films **d** 2 sccm, **e** 4 sccm, **f** 6 sccm, **g** 8 sccm, **h** 10 sccm. **i** The Raman spectra of the TiN films.

Figure 5a is the XRD pictures of TiN films at different N_2 flow rate, it can be observed that when there is a small amount of nitrogen in the sputtering process, only the spectral peak of metal Ti is detected in the film, but there is no characteristic peak of TiN. At the nitrogen flow rate of 4 sccm, the reflection peak is located at 37.4°, between the standard Ti peak and TiN, indicating that both Ti and TiN are formed in the film. For TiN films with the nitrogen fluxes between 6 and 10 sccm, only the diffraction peaks of TiN exists. As the nitrogen fluxes increases, the diffraction peaks shift to the low angle direction, indicating that there are excess N atoms entering TiN lattice, resulting in lattice expansion, which makes the characteristic peak of TiN move to the low 2θ

direction [39]. This can be explained by the results of lattice constant of TiN film, as shown in Fig. 5b. The larger the nitrogen fluxes, the larger the lattice parameters of TiN films, indicating that the lattice defects in TiN films increase [40].

Figure 5d − i shows the SEM micrographs of TiN films prepared under different N_2 fluxes. It can be noted that the surface morphology of the films is related to the amount of N_2. At the N_2 fluxes of 2 sccm, the surface morphology of large particles with an average size of 100 ∼ 200 nm (Fig. 5d). From Fig. 5e, when the N_2 flow rate is 4 sccm, the surface morphology of the film changes significantly, the particle size is greatly reduced, with an average size of 50 ∼ 60 nm. When the N_2 flow rate is 6 sccm, the

film surface presents a smooth spherical surface shape with an average size of 40 ~ 50 nm. When the N_2 flow rate is too high and greater than 6 sccm, the surface shape changes to a porous pyramid shape with an average size of 20 ~ 30 nm. The particle size on the surface of TiN film decreases with the N_2 fluxes of 8 ~ 10 sccm, indicating that the surface roughness of TiN film increases. The results of film surface roughness can also explain the changes in film surface morphology. The Ra is 13.4 nm with the N_2 flow rate of 2 sccm. The Ra on the surface of the film increased from 3.56 nm (4sccm) to 10.86 nm (10 sccm) (Fig. 5c (right axis)). The results show that the spherical and porous pyramidal particle morphology is expected to provide a larger specific surface area for TiN films and is more conducive to electron storage. From the cross section, the film thicknesses with the increase in nitrogen concentration are 668 nm, 691 nm, 626 nm, 554 nm and 452 nm, respectively.

The micromorphology of film is also one of the main factors affecting the electrical properties of TiN thin film electrode. Figure 5c (left axis) shows the change of TiN film conductivity vs. the nitrogen flow rates. The conductivity of the film is about 2687 S cm^{-1} at the nitrogen flow rate of 2 sccm. When TiN phase is formed in the film (4 sccm), the conductivity of the film is about 2316 S cm^{-1}. However, when the nitrogen flow rate is greater than 4 sccm, the conductivity of the film is greatly reduced to 475 scm^{-1} (8 sccm). Due to the transition from Ti to TiN phase and the increase in lattice defects in the film, the conductivity of the film is further reduced; With the increase of N_2 flow rate, the grain of the film is refined, resulting in the increase of the number of grain boundaries and the decrease of the conductivity of the film.

Figure 5i shows the Raman spectra of TiN films. The two Raman bands of 150 ~ 300 cm^{-1} and 400 ~ 700 cm^{-1} are caused by the first-order Raman vibration of incomplete phonons and optical phonons of TiN [41]. The vibration of heavy Ti^{4+} will cause acoustic phonons, while the vibration of light N^{3-} will cause phonons in the optical range [28]. As can be seen from Fig. 5i, the peak Raman spectrum at 210 ~ and 320 ~ can be characterized by the transverse acoustics (TA) and longitudinal acoustics (LA) of the acoustic phonon band, while the transverse optics (TO) can represent the Raman spectrum at 560 ~ [41]. When the nitrogen flow rate is

2 ~ 4sccm, the acoustic phonon part of the film is more than the optical phonon part, indicating the lack of N in the films, i.e. sub-stoichiometric, which is consistent with the XRD results. When the nitrogen content is 6 ~ 10 sccm, the optical phonon part is more than the acoustic phonon part in the Raman spectrum, indicating that the excess nitrogen exists in the films, i.e. over-stoichiometric. The intensity of optical phonons is sensitive to the content of N and increases with the increase of N content [42]. The elements content in the films analyzed by XPS is shown in Table 2.

To further clarify the chemical composition of the film surface, XPS spectroscopy was used for analysis. Table 2 shows the relative contents of Ti, N and O elements in films before erosion and after erosion for 90 s under different nitrogen flow rates. From Table 2, the films contain large amounts of O, mainly because the sample adsorbs oxygen after being taken out from the sputtering chamber. The erosion of the film surface is to remove the O adsorbed on the surface. However, the film also contains O, mainly because of the residual oxygen in the sputtering chamber and the introduction of oxygen into the mixed gas that has not been completely purified during the sputtering process. In addition, it can be seen from the element content after erosion that the content of titanium nitride in the film is closer to 1:1, which is regarded as stoichiometric TiN film when the nitrogen flow rate is 6 sccm. Therefore, the films can be divided into sub-stoichiometric TiN films (2 ~ 4 sccm), stoichiometric TiN films (6 sccm) and over-stoichiometric TiN films (8 ~ 10 sccm) according to the nitrogen flow rate.

Figures 6a, b are the Ti 2p and N 1 s fine spectra of titanium nitride films under different nitrogen flow rates (2 sccm ~ 10 sccm). From Fig. 6a, b, Similar to Fig. 4 a, b, Ti 2p has two spin peaks, Ti $2p_{1/2}$ and Ti $2p_{3/2}$. With the increase of nitrogen flow rate from 2 to 10 sccm, Ti 2p peak moves towards the direction of low binding energy, while N 1 s peak is opposite, such binding energies are typically reported for TiN compound [43]. The shape of Ti 2p spectra of the TiN films retains consistency when the nitrogen flow rate is from 6 to 10 sccm. Ti 2p can deconvolute three peaks, which are Ti−N, Ti−N–O and Ti–O, respectively. The details have been described above and will not be repeated here. For the TiN films with N_2 flow rate of 2 ~ 4 sccm, Ti 2p can be deconvoluted into four peaks, Ti–Ti, Ti−N, Ti−N–O and Ti–O. The

Table 2 The element composition of TiN film before erosion and 90 s after erosion was determined by XPS analysis

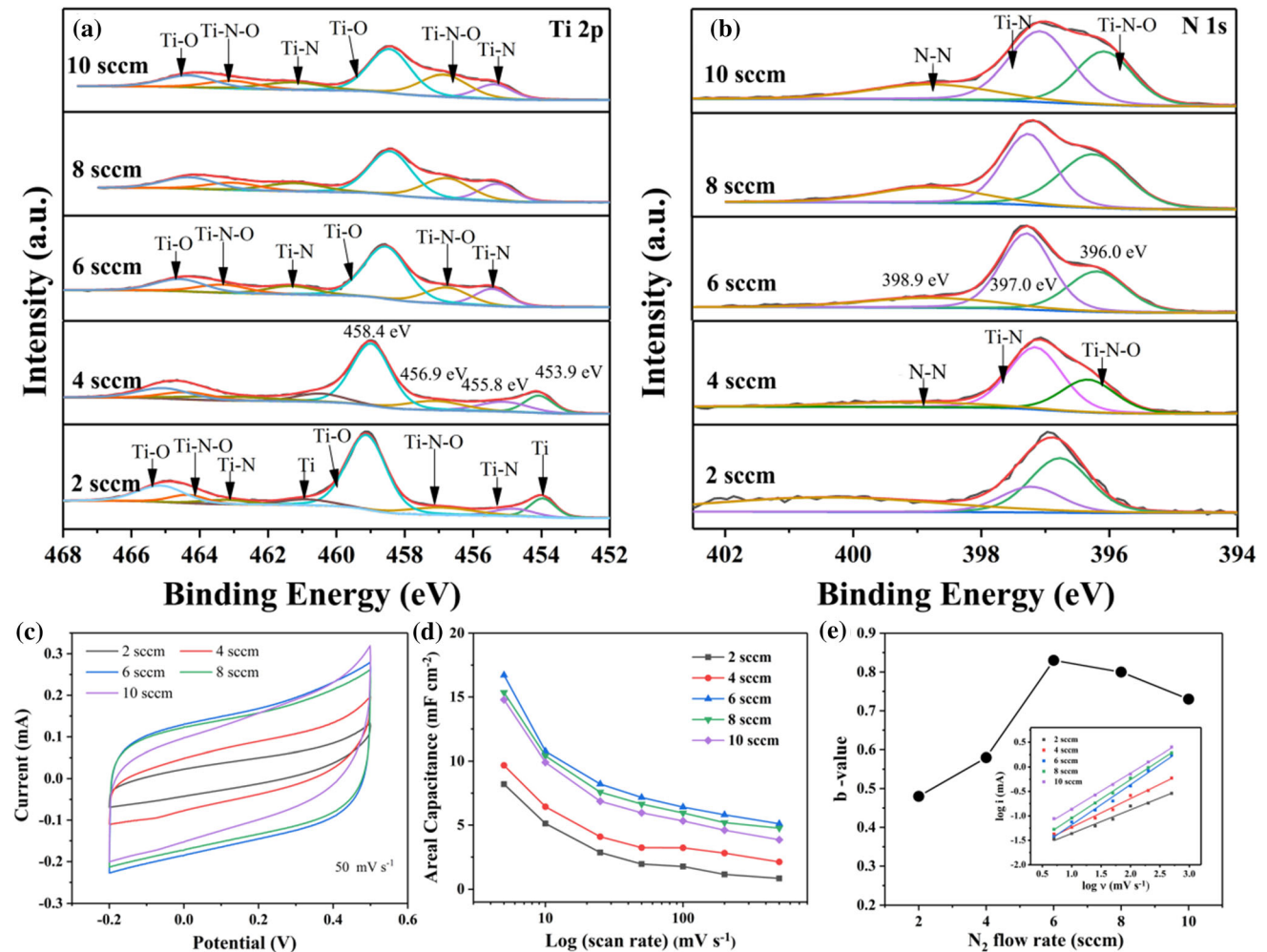| N₂ flow rate (sccm)	Before etching (at. %)			After etching (at. %)		
	Ti	N	O	Ti	N	O
2	26.67	2.42	51.17	62.15	7.85	20
4	25.37	6.89	45.45	49.45	30.2	20.35
6	23.59	19.24	37.46	37.88	38.16	22.96
8	23.94	20.06	33.59	32.24	39.25	24.79
10	22.96	18.20	35.14	30.33	40.86	24.83

Figure 6 The fine spectra of Ti 2p and N 1 s of TiN films (**a**, **b**). Electrochemical diagrams of TiN films vs. the N₂ flow rates. **c** Cyclic voltammetry curves of TiN films at a scan rate of 50 mV s⁻¹. **d** The areal capacitance of TiN films vs. log (scan rate). **e** Evolution of the b value vs. the N₂ flow rates.(Insert) the current is reported vs. the scan rate.

binding energies of 451.0 eV and 461.0 eV belong to metal bond Ti, which can obtain in substoichiomertic TiN. The existence of Ti–O and Ti−N–O in the film is mainly due to the residual oxygen in the furnace cavity and the oxygen adsorbed in the air before detection.

Table 3 shows the relative contents of four functional groups of Ti 2p deconvolution under different nitrogen flow rates (2 ~ 10 sccm). When the nitrogen flow rate is 2 ~ 4 sccm, the film contains a large amount of Ti, which is good consistent with the XRD results. When the nitrogen flow rate is 6 ~ 10 sccm, the nitrogen ionization was sufficient in the

Table 3 The composition of chemical bonds of the deconvoluted peaks from XPS speatra

N$_2$ flow rate (sccm)	Deconvoluted peaks from XPS spectra						
	Ti 2p				N 1 s		
	Ti	Ti − N − O	Ti − N	Ti − O	Ti − N − O	Ti − N	N − N
2	23.71	23.21	23.77	29.31	35.17	32.07	32.76
4	24.05	23.99	24.04	27.92	33.03	35.81	31.16
6	0	33.80	30.14	36.06	35.88	35.55	29.57
8	0	32.03	32.72	35.25	33.34	35.46	31.2
10	0	31.78	32.93	35.29	33.67	32.81	33.52

sputtering process, and no XPS characteristic peak of Ti was found. The contents of Ti–O and Ti−N–O in the films first increased (2 ∼ 6 sccm) and then decreased (6 ∼ 8 sccm) with the increase in nitrogen flow rate. When the nitrogen flow rate was 6 sccm, the relative contents of chemical bonds of Ti−N–O and Ti–O were the highest at 33.80% and 36.06% respectively. The increase of Ti−N–O bonds can promote the charge storage on the electrode.

Figure 6c describes the CV curves of films with different nitrogen flow rates in 0.5 M K$_2$SO$_4$ solution. From the figure, the CV curves of TiN electrodes with a nitrogen flow of 6 ∼ 10 sccm are approximately rectangular, indicating that the TiN film electrodes have quasi ideal capacitance behavior. However, with the increase in nitrogen flow rate, the areal capacitance of the film decreases. The film with a nitrogen flow of 6 ∼ 8 sccm has good capacitance retention, while when the scanning speed is greater than 100 mV s^{-1}, the capacitance retention of the film with nitrogen flow of 10 sccm decreases. This is attributed to the decrease the TiO$_x$N$_y$ on the surface of the over-stoichiometric film with the increase of nitrogen flow (8 ∼ 10 sccm), which is related to the decrease of pore size of the film surface. If the average pore size is too small, ions/cations cannot pass through this pore, reducing the areal capacitance of the over-stoichiometric film [44]. The sub-stoichiometric films with a nitrogen flow of 2 ∼ 4 sccm have fewer capacitance due to less surface electroactive substances TiN and nitrogen oxides. When the nitrogen flow rate is 10 mV s^{-1}, the areal capacitance of titanium nitride thin film electrode is 5.13, 6.44, 10.77, 10.42 and 9.90 mF cm^{-2}, respectively (Fig. 6d). The stoichiometric TiN membrane electrode with a nitrogen flow of 6 sccm has the largest specific surface area, due to the large pore size of the film

surface, and the pseudocapacitive active substances, which all promote TiO$_x$N$_y$ on the film surface.

The electrochemical kinetic analysis shows that the stoichiometric TiN film electrode (6 sccm) and over-stoichiometric thin film electrodes (8 ∼ 10 sccm) mainly store charge through capacitance (Fig. 6e). The sub-stoichiometric titanium nitride film electrodes are mainly diffusion types.

Influence of thickness

Deposition pressure and nitrogen flow rate are the key parameters to adjust the porosity and surface chemical composition of titanium nitride films. However, to further improve the areal capacitance of the film electrode, the thickness of the TiN film was changed while maintaining a constant voltage and nitrogen flow to achieve this goal. When the deposition pressure is 0.98×10^{-3} torr, the nitrogen flow rate is 6 sccm, and other parameters remain unchanged, the sputtering time of the film is controlled to change the thickness of the film.

Figure 7a displays the XRD patterns of TiN films at different deposition times. From the figure, the TiN film has four TiN peaks, which are (111) (200) (220) (311) respectively, and the density of TiN (111) peak becomes stronger with the increase in film thickness. The reflection peaks of other TiN hardly changed.

Figure 7d–h shows the surface of TiN film at different deposition times. It can be seen from the surface morphology that the surface of TiN film is granular or spherical, the size of particle agglomeration increases with the increase in thickness, and large pores appear on the surface. This is mainly due to the grain growth caused by the increase of furnace temperature during the long-time sputtering. In addition, the surface morphology of TiN films deposited for a long time (2 h, 3 h) has little change. The corresponding film thicknesses of TiN films
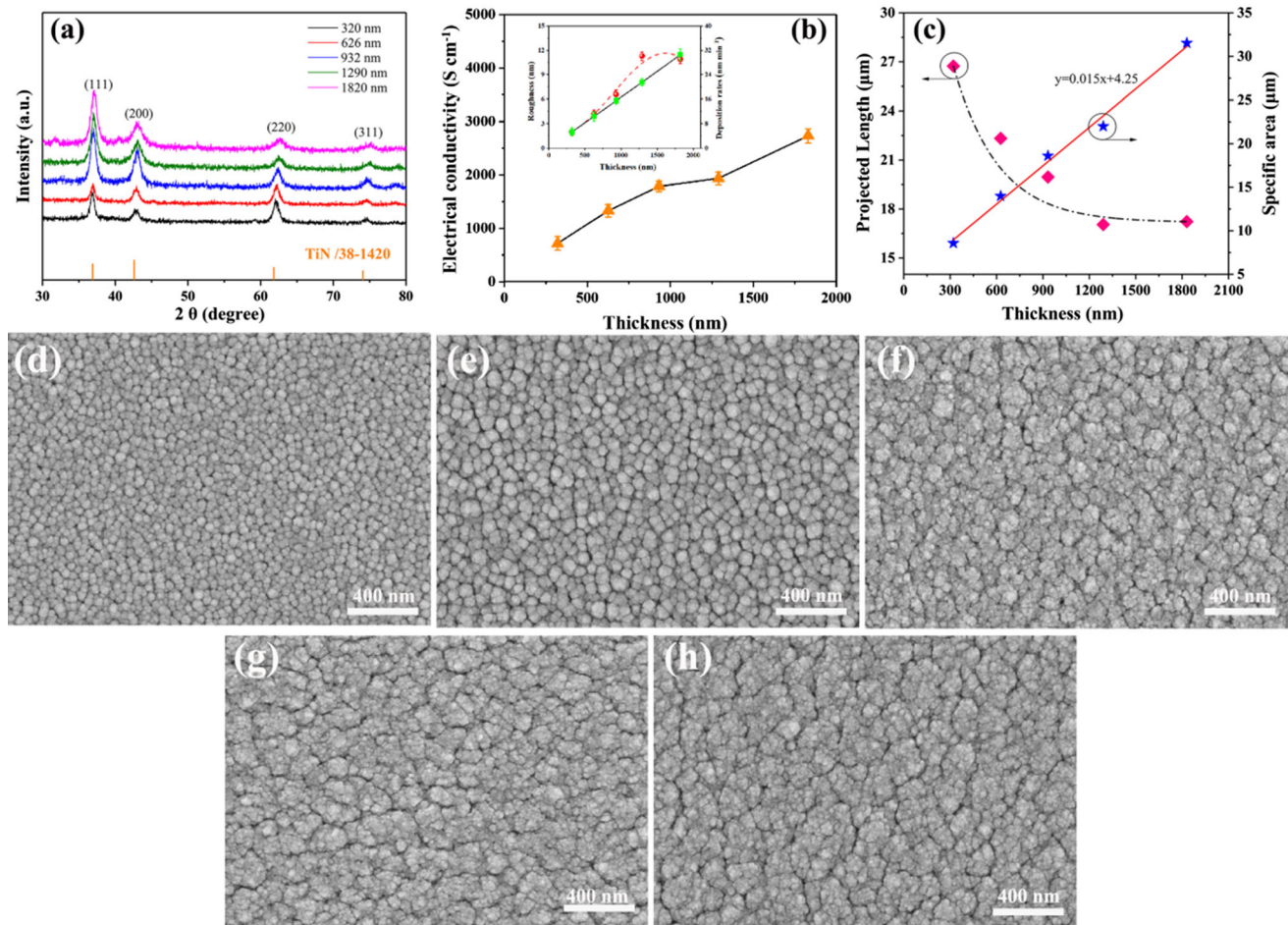
Figure 7 XRD patterns of TiN films (**a**). **b** Variation of Electrical conductivity vs. the thicknesses. (Insert) Evolution of the roughness and thickness vs. the thickness. **c** Variation of S_e and L_p with thickness. The surface and cross morphologies of the TiN films vs. the thickness: **d** 320 nm, **e** 626 nm, **f** 932 nm, **g** 1290 nm, **h** 1820 nm.

deposited for 0.5, 1, 1.5, 2 and 3 h are 320, 626, 932, 1290 and 1830 nm, respectively. This is the result of an almost linear increase in TiN film deposition rate with the increase of sputtering time (Fig. 7b (right axis) insert).

Figure 7b shows the conductivity of TiN films with different thicknesses. The conductivity of TiN films with different thickness increases with the increase in thickness. Specifically, the conductivity of TiN films with a thickness of 320 nm increases from 719.5 to 2732 S cm^{-1} with a thickness of 1820 nm. This is related to the better crystallinity of TiN films with increasing thickness (Fig. 7a). In addition, as the film thickness increases, the particle size on the film surface increases, and the interface between the film particles decreases, resulting in the increase of the conductivity of the film.

Figure 7b left axis (Insert) shows the root mean square roughness (Ra) of TiN films with different thicknesses. With the increase of TiN film thickness from 320 to 1830 nm, the surface roughness values of TiN are 2.03 nm, 4.46 nm, 6.56 nm, 11.30 nm and 10.9 nm, respectively. The roughness of TiN film increases sharply with the increase of thicknesses and then slows down, indicating that the dependence of roughness on thick film is weakened. This corresponds well to the surface morphology of TiN films.

The thickness of TiN film has a great influence on the surface roughness of the film. What is the dependence of film thickness on a specific surface area (S_e)? The specific surface area of TiN films with different thickness is determined by image analysis technology [27, 35]. Where L_P is the maximum length of particle, defined as the projection length. The ratio of a given height to the total height of the grain is
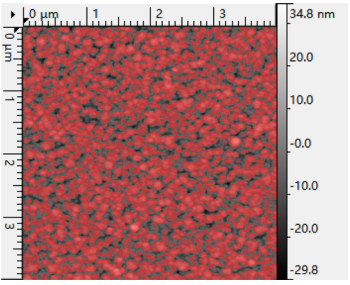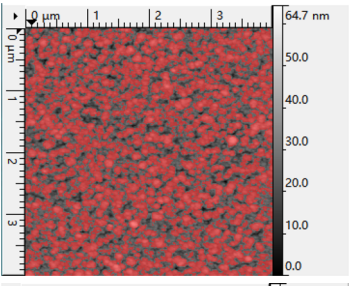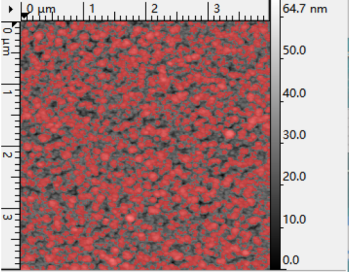
Table 4 Projection length determination method

Mask threshold (%)	Illustration of the selected grains	Projected length (microns)
42		293.2
44		304.2
46		303.1

Table 5 The average values of L_p S_e of the TiN films with different thicknesses

Thickness (nm)	L_p (μm)	S_e (cm^2)
320	26.74	8.58
626	22.33	13.99
932	19.96	18.60
1290	17.05	22.00
1830	17.23	31.53

called the masking threshold. The maximum perimeter of the projection of the grain on the mask is obtained by moving the mask. An example of a 932 nm TiN film L_p (4×4 μm^2) is given in Table 4. The L_p values of other TiN films are shown in Table 5. From Table 5, the L_p value first decreases and then tends to be stable with the increase of thickness. Specifically, the L_p value decreases from 26.74 nm (320 nm) to 19.96 μm (932 nm). When the film

thickness is greater than 932 nm, the value tends to be about 17.5 μm.

If the square (side length a) of the scan area is filled with circular particles of radius r, the total perimeter of the particles in the selected square area is is calculated as formula (4), (5):

$$N = a^2/4r^2 \tag{4}$$

$$L_p = 2\pi r \times N = \pi a^2/2r \tag{5}$$

N is the number of grains. Since L_p is inversely proportional to the particle radius, L_p decreases with the increase of particles (SEM), that is, with the increase of film thickness, which is consistent with the L_p results calculated by image analysis technology, as shown in Fig. 7b (left axis). Since the specific surface of the film is represented by the product of L_p and film thickness (h), i.e. $S_e = L_p \times h$. The change results of film thickness and film S_e are obtained through calculation, as shown on the right axis of Fig. 7c. As the film thickness increased from 320 to
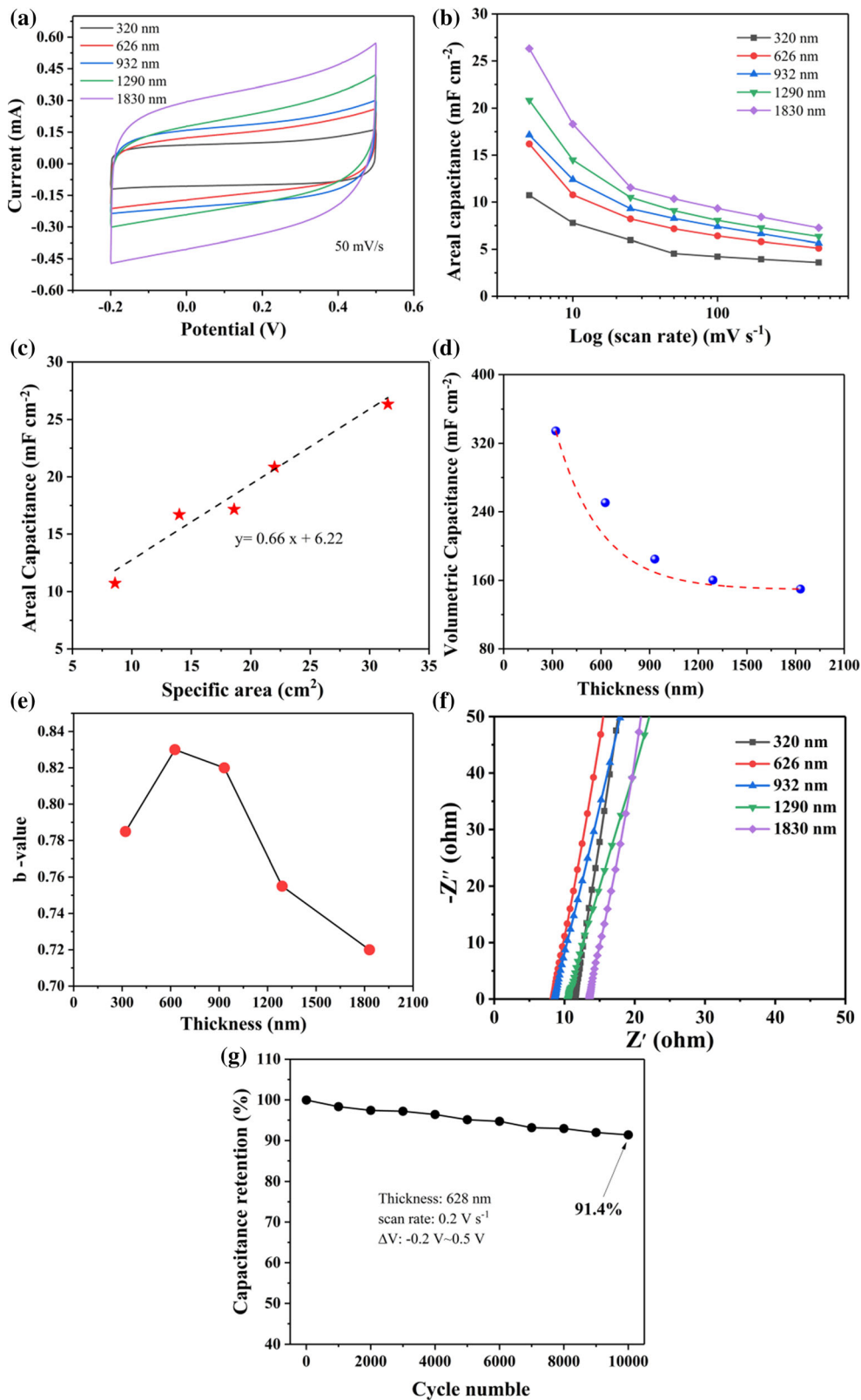
◂**Figure 8** Cyclic voltammetry curves vs. thickness at 50 mV s^{-1} (**a**). **b** Relationship between areal capacitance and log(scan rate) of thin-film electrodes with different thicknesses. **c** Variation of S_e and L_p with thickness. **d** The volumetric capacitance of TiN films vs. the thickness. **e** Variation of the b value vs. the thickness. **f** Nyquist plots of TiN film electrodes vs. the thicknesses. **g** Cycling stability test of the film electrode with 626 nm at of 200 mV s^{-1}.

1830 nm, the S_e of the film surface increased from 8.58 to 31.53 cm^2 per cm^2. The specific surface area of the film increases linearly as a function of y = 0.015x + 4.25. The results show that increasing the thickness of the film can increase the S_e of the film. According to the L_p values in different regions, the average L_p and S_e of TiN films with different thicknesses were calculated, as shown in Table 5.

To further clarify the relationship between the specific surface area of different films and the areal capacitance of film electrodes. Figure 8 shows the electrochemical curves of films with different thicknesses. Figure 8a, b is the CV curves of the film electrodes and the calculated areal capacitance. It can be seen from the figure that the areal capacitance of the film increases with the increase of thickness. When tested at 10 mV s^{-1}, the areal capacitance of the TiN film electrode increased from 5.34 mF cm^{-2} with a thickness of 320 to 14.31 mF cm^{-2} with a thickness of 1830 nm. In addition, it is observed from Fig. 8c that there is a good correlation and linear relationship between the specific surface area of the film extracted from the AFM measurement and the measured areal capacitance (Fig. 8c) (5 mV s^{-1}). The results show that the areal capacitance has a linear relationship with the specific surface area of the TiN film. Specifically, when the S_e increases from 8.58 cm^2 (320 nm) to 31.53 cm^2 (1830 nm), the areal capacitance of TiN increases from 10.73 to 26.32 mF cm^{-2}. The areal capacitance and the specific surface of the film follow the linear relationship of y = 0.66x + 6.22. The significant increase in areal capacitance is mainly due to the increase in load and surface area. It is observed in Fig. 8d that the volume capacitance of the film does not depend on the film thickness, but will drop to a constant value of 175 F cm^{-3} once the thickness is greater than 932 nm (Fig. 8d). The change in volume capacitance is mainly related to the increase in film contact resistance. The

electrochemical kinetics of TiN films with different thicknesses are explained below.

The b-value was extracted from the CV experiment as a function of thickness to reflect the electrochemical kinetics of TiN thin film electrode storage. As for the evolution of surface capacitance of 320 ~ 1830 nm thick films at 5 ~ 500 mV s^{-1}. It is observed from Fig. 8e that when the thickness is increased from 320 to 628 nm, the b value increases slightly. For the thicker layer, the b value decreases from 0.83 to 0.72, indicating that the thicker film surface gradually shows a diffusion control process. It can also be seen from the EIS diagram of the film that all films are perpendicular to the X-axis (Fig. 8f), which is closer to the ideal capacitor. The contact resistance increases with the film thickness, facilitating the diffusion of thicker films. The contact resistance of TiN film electrodes with different thicknesses are 11.4, 8.4, 10.2, 11.6 and 14.1 Ω, respectively, corresponding to 320, 626, 932, 1290 and 1830 nm. This shows that the film thickness of 628 nm has a superior electrochemical property.

Figure 8g exhibits the areal capacitance retention of 626 nm TiN film electrodes obtained from CV curves. After 10,000 cycles with K_2SO_4, the retention capacity of the TiN electrode is 91.4%, which confirms the TiN film electrode with 626 nm displays excellent cycling performance.

The adhesion between thin film and substrate is one of the important factors to measure the cyclic stability of thin film electrode. Figure 9 is a photo of the scratch morphology of films with different thicknesses. The area marked in the white box in figure is the location of the initial cracking and spalling of the film. At this time, the corresponding load is the critical load, as shown in Fig. 10. It can be seen from the Fig. 10 that when the film thickness is 320 nm ~ 626 nm, the film has high adhesion and large critical load (30 N), and the scratch of the coating is complete and the morphology is long. However, with the increase of the film thickness, the adhesion of the film is small, and the film fracture will occur soon. The reason for the poor adhesion of thick film is that the substrate is not biased to increase the specific surface area of the film.

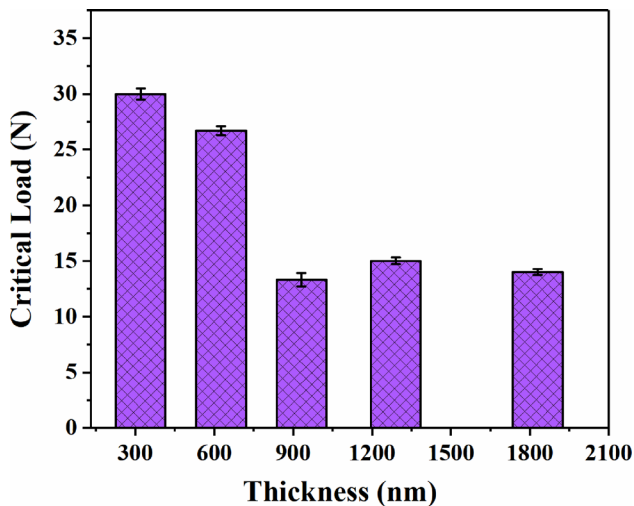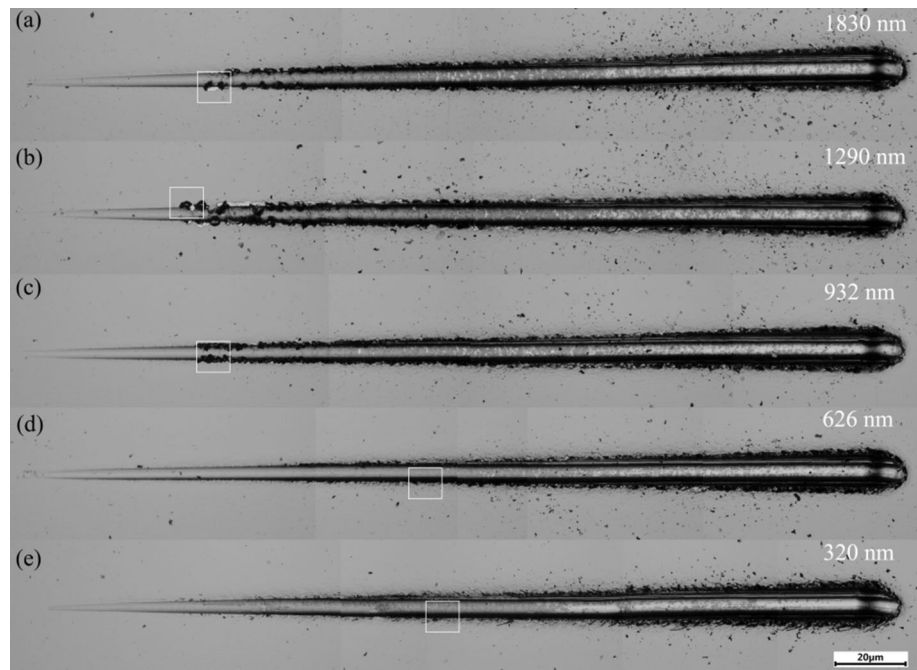**Figure 9** Metallographic micrographs of scratches on films of different thickness.

Figure 10 Critical load of films with different thickness.

Conclusion

In this paper, TiN thin film electrodes were produced by a reactive magnetron sputtering method. The main conclusions are:

1. Higher working pressure reflected more porosity and the better the electrochemical performance of the corresponding TiN film.
2. Stoichiometric films and over-stoichiometric TiN films had a larger areal capacitance than sub-stoichiometric films. The electrochemical storage behavior differed by the large pore size on the film surface and the formation of more TiO_xN_y on the surface.
3. The specific surface area of the TiN film was linearly related to the areal capacitance of $y = 0.66x + 6.22$. In addition, the volume capacitance is independent of the film thickness, and when the film thickness was greater than 932 nm the volume capacitance falls to a constant value of 175 F cm^{-3}.
4. The bifunctional TiN film electrode with a thickness of 626 nm had excellent cycling performance, which can cycle 10,000 times in K_2SO_4 electrolyte solution, and the holding areal capacitance is still 91.4%.

These studies show that titanium nitride film is a suitable bifunctional material, which opens up a new prospect for exploring the electrochemical storage applications of other transition metal nitride electrodes. However, the surface of TiN film electrodes prepared by changing sputtering parameters is still relatively flat. In order to obtain higher performance TiN film electrodes, future research work can be carried out in the following aspects: (1) The specific surface area of TiN film electrode can be further improved by the method of nanocrystallization of substrate structure; (2) The comprehensive properties of TiN films can be improved by engineering doping.

Authors contribution

JS: Data curation, Investigation, Methodology, Writing—original draft. BJ: Conceptualization, Supervision, Writing—review and editing, Resources. CL: Software, Visualization, Investigation. ZL: Supervision, Validation, Writing—review and editing. FY: Software, Visualization, Investigation. TW: Methodology, Supervision. JH: Visualization, Investigation. DD: Supervision, Software, Validation.

Declaration

Conflict of interest

The authors declare that they have no known competing financial interests or personal relationships that could have appeared to influence the work reported in this paper.

References

[1] Wang ZL (2012) Self-powered nanosensors and nanosystems. Adv Mater 24:280–285

[2] Kim H, Shaqeel A, Han S, Kang J, Yun J, Lee M (2021) In Situ Formation of Ag nanoparticles for fiber strain sensors: toward textile-based wearable applications. ACS Appl Mater Inter 13:39868–39879

[3] Liao XQ, Wang WS, Wang L, Jin HR, Shu L, Xu XM (2021) A highly stretchable and deformation-insensitive bionic electronic exteroceptive neural sensor for human-machine interfaces. Nano Energy 80:105548

[4] Armand M, Tarascon JM (2008) Building better batteries. Nature 451:652–657

[5] Yu FK, Chen Y, Pan YW, Yang Y (2020) A cost-effective production of hydrogen peroxide via improved mass transfer of oxygen for electro-Fenton process using the vertical flow reactor. Sep Purif Technol 241:116695

[6] Lewis N, Nocera D (2018) Powering the planet: Chemical challenges in solar energy utilization. P Natl Acad Sci USA 103:15729–15735

[7] Liu CL, Bai Y, Wang J (2021) Controllable synthesis of ultrathin layered transition metal hydroxide/zeolitic imidazolate framework-67 hybrid nanosheets for high-performance supercapacitors. J Mater Chem A 9:11201–11209

[8] Zheng S, Li Q, Xue H (2020) A highly alkaline-stable metal oxide@ metal-organic framework composite for high-performance electrochemical energy storage. Natl Sci Rev 7:305–314

[9] Liu CL, Bai Y, Li WT, Yang FY, Zhang GG, Pang H (2022) In Situ growth of three-dimensional MXene/Metal-Organic framework composites for high-performance supercapacitors. Angewandte Chemmie 7:e202116282

[10] Bai Y, Liu C, Chen T, Li W, Zheng S (2021) MXene-copper/cobalt hybrids via lewis acidic molten salts etching for high performance symmetric supercapacitors. Angewandte Chemmie 133:25522–25526

[11] Zheng S, Sun Y, Xue H, Braunstein P (2021) Dual-ligand and hard-soft-acid-base strategies to optimize metal-organic framework nanocrystals for stable electrochemical cycling performance. Nat Sci Rev

[12] Yang Z, Xu F, Zhang W, Mei Z, Pei B, Zhu X (2014) Controllable preparation of multishelled NiO hollow nanospheres via layer-by-layer self-assembly for supercapacitor application. J Power Sources 246:24–31

[13] Huang YL, Zeng YX, Yu MH, Liu P, Tong YX, Cheng FL, Lu XH (2018) Recent smart methods for achieving high-energy asymmetric supercapacitors. Small Methods 2:1700230

[14] Bahari Y, Mortazavi B, Rajabpour A et al (2021) Application of two-dimensional materials as anodes for rechargeable metal-ion batteries: a comprehensive perspective from density functional theory simulations. Energy Storage Mater 35:203–282

[15] Makaremi M, Mortazavi B, Rabczuk T et al (2018) Theoretical investigation: 2D N-graphdiyne nanosheets as promising anode materials for Li/Na rechargeable storage devices. ACS Appl Nano Mater 2:127–135

[16] Zhang X, Zhang H, Lin Z, Yu M, Lu X, Tong Y (2016) Recent advances and challenges of stretchable supercapacitors based on carbon materials. Sci China Mater 59:475–494

[17] Huang M, Zhang Y, Li F, Zhang L, Wen Z, Liu Q (2014) Facile synthesis of hierarchical Co_3O_4@MnO_2core-shell arrays on Ni foam for asymmetric supercapacitors. J Power Sources 252:98–106

[18] Simon P, Gogotsi Y (2008) Materials for electrochemical capacitors. Nat Mater 7:845–854

[19] Zhou X, Shang C, Gu L, Dong S, Chen X, Han P, Li L, Yao J (2011) Mesoporous coaxial titanium nitride-vanadium nitride fibers of core-shell structures for high-performance supercapacitors. ACS Appl Mater Interfaces 3:3058–3063

[20] Lu XH, Wang GM, Zhai T, Yu MH, Xie SL (2012) Stabilized TiN nanowire arrays for high-performance and flexible supercapacitors. Nano Lett 12:5376–5381

[21] Achour A, Lucio-Porto R, Chaker M (2017) Titanium vanadium nitride electrode for micro-supercapacitors. Electrochem Commun 77:40–43

[22] Dong S, Chen X, Gu L, Zhou X, Xu H, Wang H, Liu Z et al (2011) Facile preparation of mesoporous titanium nitride microspheres for electrochemical energy storage. Appl Mater Interfaces 3:93–98

[23] Qin P, Li X, Gao B, Fu J, Xia L, Zhang X, Huo K, Shen W, Chu P (2018) Hierarchical TiN nanoparticles-assembled nanopillars for flexible supercapacitors with high volumetric capacitance. Nanoscale 10:8728–8734

[24] Hou X, Li Q, Zhang L, Yang T (2018) Tunable preparation of chrysanthemum-like titanium nitride as flexible electrode materials for ultrafast-charging/discharging and excellent stable supercapacitors. J Power Sources 396:319–326

[25] Dong S, Chen X, Gu L, Zhou X, Wang H, Liu Z, Han P, Yao J, Wang L, Cui G, Chen L (2011) Facile preparation of mesoporous titanium nitride microspheres for electrochemical energy storage. Mater Res Bull 46:835

[26] Kyeremateng NA, Brousse T, Pech D (2017) Microsupercapacitors as miniaturized energystorage components for on-chip electronics. Nat Nanotechnol 12:7–15

[27] Ouendi S, Robert K, Stievenard D, Brousse T, Roussel P, Lethien C (2019) Sputtered tungsten nitride films as pseudocapacitive electrode for on chip micro-supercapacitors. Energy Storage Mater 20:243–252

[28] Liu XH, Zhou DY, Guan Y, Li SD, Cao F, Dong XL (2018) Endurance properties of silicon-doped hafnium oxide ferroelectric and antiferroelectric-like thin films: a comparative study and prediction. Acta Mater 154:190–198

[29] Sun NN, Zhou DY, Liu WW, Zhang Y, Li SD, Wang JJ (2020) Importance of tailoring the thickness of SiO_2 interlayer in the observation of ferroelectric characteristics in yttrium doped HfO_2 films on silicon. Vacuum 8:109835

[30] Achour A, Porto RL, Soussou MA, Islam M (2015) Titanium nitride films for micro-supercapacitors: Effect of surface chemistry and film morphology on the capacitance. J Power Sources 300:525–532

[31] Achour A, Chaker M, Achour H, Arman A, Islam M, Mardani M et al (2017) Role of nitrogen doping at the surface of titanium nitride thin films towards capacitive charge storage enhancement. J Power Sources 359:349–354

[32] Sun N, Zhou D, Liu W et al (2021) Sputtered titanium nitride films with finely tailored surface activity and porosity for high performance on-chip micro-supercapacitors. J Power Sources 489:229406

[33] Sun N, Zhou D, Liu W et al (2020) Tailoring surface chemistry and morphology of titanium nitride electrode for on-chip supercapacitors. ACS Sustain Chem Eng 8(21):7869–7878

[34] Bleu Y, Barnier V, Christien F, Bourquard F (2019) Dynamics of carbon diffusion and segregation through nickel catalyst, investigated by in-situ XPS, during the growth of nitrogen-doped graphene. Carbon 155:410–420

[35] Shi J, Jiang BL, Liu Z, Li C ((2021)) Effects of specific surface area of electrode and different electrolyte on capacitance properties in nano porous-structure CrN thin film electrode for supercapacitor. Ceram Int 47:18540–18549

[36] Barna PB, Adamik M (1998) Fundamental structure forming phenomena of polycrystalline films and the structure zone models. Thin Solid Films 317:27–33

[37] Sun N, Xu J, Zhou D, Zhao P, Li S (2018) DC reactively sputtered TiN_x, thin films for capacitor electrodes. J Mater Sci Mater Electron 29:10170–10176

[38] Zhang Y, Li L, Su H et al (2015) Binary metal oxide: advanced energy storage materials in supercapacitors. J Mater Chem A 3(1):43–59

[39] ShenYG, Mai YW (2000) Effect of oxygen on residual stress and structural properties of tungsten nitride films grown by reactive magnetron sputtering. Mater Sci Eng B Solid State Mater Adv Technol 76:107–115

[40] Baker CC, Shah SI (2002) Reactive sputter deposition of tungsten nitride thin films. J Vac SciTechnol A Vac Surf Film 20:1699–1703

[41] Ding ZH, Yao B, Qiu LX, Lv TQ (2006) Raman scattering investigation of nanocrystalline δ-TiN_x synthesized by solid-state reaction. J Alloys Compd 421:247–251

[42] Chen C, Liang N, Tse W, Chen I, Duh J (1994) Raman spectra of titanium nitride thin Films. Chin J Phys 32:205–210

[43] Shi J, Jiang BL, Liu Z, Li C (2021) Sputtered titanium nitride films on nanowires Si substrate as pseudocapacitive electrode for supercapacitors. Ceram Int 47:26758–26767

[44] Heon M, Lofland S, Applegate J, Nolte R, Cortes E, Hettinger JD, Taberna PL (2011) Continuous carbide derived carbon films with high volumetric capacitance. Energy Environ Sci 4:135–138